David Tomás Sánchez Martínez
Lourdes García Rodríguez
(coordinadores)

Proceedings of the 7th International Seminar on ORC Power Systems

Editorial Universidad de Sevilla

Proceedings of the 7th International Seminar on

ORC

Power Systems

David Tomás Sánchez Martínez
Lourdes García Rodríguez
(coordinadores)

Proceedings of the 7th International Seminar on

ORC
Power Systems
(ORC2023)

4th to 6th
SEPTEMBER
SEVILLE 2023

EDITORIAL
UNIVERSIDAD DE SEVILLA

Sevilla, 2024

Colección Actas
Núm.: 91

c/ Porvenir, 27 - 41013 Sevilla.
Tlfs.: 954 487 447; 954 487 451; Fax: 954 487 443
Correo electrónico: info-eus@us.es
Web: https://editorial.us.es

ISBN 978-84-472-2745-7
DOI: https://dx.doi.org/10.12795/9788447227457

Diseño de cubierta y maquetación: los autores

INDEX OF CONTRIBUTIONS

SEVILLE 2023
7th International Seminar on O.R.C. Power Systems

DOI: https://dx.doi.org/10.12795/9788447227457_48

Pressure profile optimisation of a nozzle for wet-to-dry expansion

Pawel Ogrodniczak[1,*], Abdulnaser Sayma[1], Martin T. White[1,2]

[1] *City, University of London, Northampton Square, London EC1V 0HB, United Kingdom*
[2] *University of Sussex, Falmer, Brighton BN1 9RH, United Kingdom*

*Corresponding Author: pawel.ogrodniczak@city.ac.uk

ABSTRACT

Wet-to-dry expansion within the nozzle guide vane of an ORC turbine has been proposed as a means to improve the power output of ORC systems for waste-heat recovery (< 250 °C). However, given the rapid fluid acceleration in the stator, the phases can develop significant velocity and temperature disparity due to the density difference and finite rate of interphase heat transfer. Since these factors can significantly affect the phase-change process, wet-to-dry nozzle design techniques must account for non-equilibrium effects. The first part of this paper aims to further validate a previously developed quasi-1D inviscid nozzle design tool that accounts for non-equilibrium effects. The interphase mass, momentum and energy exchange models have been updated using correlations better tailored to evaporating droplet flows, while the drag equation and vapour mass fraction definition have been updated. The validation is performed using non-equilibrium CFD simulations, which, unlike the design model, account for lateral flow variations, viscous and turbulence effects, and secondary momentum forces. The results showed that these effects delay the evaporation, with CFD-predicted outlet vapour mass fraction being about 10 to 15% smaller than predicted by the quasi-1D tool. However, the overall flow behaviour and phase-change pattern were in satisfactory agreement, justifying the use of the design tool for 1D optimisation. In the second part of the paper, the quasi-1D tool is coupled to a gradient-based optimiser to optimise the nozzle pressure profile and enhance evaporation of siloxane MM for expansions with inlet pressure ranging from 450 to 650 kPa, and inlet quality of 0.3. The design variables are the control points of a Bezier curve that defines the shape of the intended nozzle pressure profile. CFD simulations of the optimised geometries indicate a 5.5 to 6.6% increase in the outlet vapour mass fraction, which was raised from 84.9, 88.2 and 90.7% to 90.4, 94.8 and 97.2% for the 450, 550 and 650 kPa inlet pressures respectively. More abrupt expansion in the optimised nozzles resulted in the development of a shock and led to nozzle efficiency deterioration compared to the baseline. This emphasises the need for multi-objective optimisation, which will be conducted in future studies.

1 INTRODUCTION

In an effort to improve the performance of ORC systems, researchers have proposed several novel cycle architectures (Wieland et al., 2023). Among the proposed alternatives, the so-called wet-to-dry cycle could be capable of generating up to 30% more power than the basic single-phase ORC in the temperature range between 150 and 250 °C (White, 2021). In the wet-to-dry cycle, a two-phase working fluid can completely vapourise during expansion, in the process referred to as flash boiling. This offers greater flexibility in terms of expander selection than other two-phase cycles; turbomachines could be employed provided that complete mixture evaporation occurs in the stator, thus avoiding possible concerns related to erosion in the rotor. Turbomachines offer higher expansion ratios than volumetric expanders, enabling application of the wet-to-dry cycle at temperatures above 150 °C. Moreover, having a turbine that could accept two-phase inlet conditions could be an advantage in the off-design operation of ORC systems (Lhermet et al., 2022).

The successful design of a wet-to-dry turbine depends on the capability of the stator to facilitate complete mixture evaporation to avoid liquid droplets entering the rotor. Preliminary numerical studies, using simplified equilibrium models, indicate a radial turbine stator can be designed that can facilitate the wet-to-dry transition (White, 2021). Further investigations have demonstrated that more realistic flow modelling techniques that account for mechanical and thermal non-equilibrium between the liquid and vapour phases are required when assessing the evaporation process under conditions relevant to the wet-to-dry cycle (White, 2022). Later investigations focused on non-equilibrium CFD simulations in a simple converging-diverging nozzle, demonstrating that full evaporation may be difficult to achieve in a nozzle with low inlet pressures (Ogrodniczak & White, 2023), although low pressures are more attractive from the standpoint of maximising cycle performance (White, 2021). However, these previous investigations assumed a fixed nozzle pressure distribution and did not consider any form of geometry optimisation.

This study aims to optimise the pressure profile in a converging-diverging nozzle, having a straight centerline (non-deflecting nozzle), seeking to maximise evaporation rate of two-phase siloxane MM. To this end, a previously developed quasi-1D non-equilibrium two-phase nozzle design tool was employed (White 2022). The design tool has been updated to make it more suitable for evaporating droplet flows and then verified using non-equilibrium CFD simulations. It is important to note that the tool assumes a quasi-1D inviscid flow, which means that neither lateral phase separation nor viscosity effects could be considered during optimisation. Phase separation (e.g. liquid film forming in the vicinity of the nozzle wall) could reduce the available contact area between the phases, which in turn leads to reduced interphase heat and mass transfers, and lower evaporation rates. Moreover, in the context of two-phase turbines, phase separation in the stator would be associated with flow non-uniformities at the rotor inlet and possible erosion issues. As for the effect of viscosity, it is mainly responsible for entropy generation; thus, the quasi-1D inviscid model cannot simultaneously estimate the vapourisation rate and nozzle performance. Although the above effects are not considered at the optimisation stage, the optimised geometries are simulated using two-dimensional CFD, which accounts for the phase lateral separation as well as the effects of viscosity and turbulence, serving a means of validation and providing an expanded analysis. The results reveal the influence of the pressure profile and nozzle shape on the evaporation rate, nozzle performance and flow behaviour.

2 QUASI-1D NOZZLE DESIGN TOOL VALIDATION

2.1 Two-fluid Model

305

This section provides an overview of the two-fluid model that is employed in both the quasi-1D nozzle design tool and the CFD simulations. It also highlights the modifications that have been introduced in this study to tailor the model to evaporating droplet flows. For more detailed information, an interested reader is referred to our previous work (White 2022; Ogrodniczak & White, 2022, 2023).

Flash boiling in the nozzle is simulated using the two-fluid model, also known as the six-equation model. The two-fluid model employs the Eulerian-Eulerian framework to analyse the two-phase flow, which means that both phases are treated as interpenetrating continua, with separate conservation equations:

$$\frac{\partial(\alpha\,\rho)_\beta}{\partial t} + \nabla\cdot\left(\alpha\,\rho\,\vec{U}\right)_\beta = \dot{m}_{ex} \tag{1}$$

$$\frac{\partial\left(\alpha\,\rho\,\vec{U}\right)_\beta}{\partial t} + \nabla\cdot\left(\alpha\,\rho\,\vec{U}\,\vec{U}\right)_\beta = -\alpha_\beta\,\Delta P + \nabla\cdot\tau_\beta + \dot{m}_{ex}\,\vec{U}_{ex} + M_{ex} \tag{2}$$

$$\frac{\partial(\alpha\,\rho\,h_{tot})_\beta}{\partial t} + \nabla\cdot\left(\alpha\,\rho\,\vec{U}\,h_{tot}\right)_\beta = -\alpha_\beta\frac{\partial P}{\partial t} + \nabla\cdot(\alpha\,\lambda\,\Delta T)_\beta + \nabla\cdot\left(\vec{U}\,\tau\right)_\beta + \dot{m}_{ex}\,h_{ex} + \dot{q}_{ex} \tag{3}$$

where β is the phase index, α the volume fraction, ρ the density, $\vec{U}$ the velocity vector, P the pressure (assumed identical in both phases), τ the stress tensor, while h_{tot}, T and λ are specific total enthalpy, temperature and thermal conductivity. The volume fraction conservation equation is also solved, which states that the sum of phase volume fractions equals unity. The phases interact by exchanging mass, momentum and energy. The interphase mass exchange is denoted by $\dot{m}_{ex}$, and the products $\dot{m}_{ex}\,\vec{U}_{ex}$ and $\dot{m}_{ex}\,h_{ex}$ represent the interphase exchange of momentum and energy associated with the mass transfer. The additional momentum and energy exchange terms are the interfacial forces and heat-exchange, which are denoted as M_{ex} and $\dot{q}_{ex}$ respectively. The phase change is assumed to be solely the result of interphase heat transfer, which is evaluated by means of a two-resistance model. The two-resistance model assumes an interface between the phases, which is at local saturation temperature. Vapour and liquid exchange heat with the interface, and the sum of heat exchanged across the interface determines the interphase mass transfer:

$$\dot{m}_{ex} = \frac{\dot{q}_{ex}}{h_L - h_V} = \frac{\mathfrak{H}_L A_{int}(T_{int} - T_L) + \mathfrak{H}_V A_{int}(T_{int} - T_V)}{h_L - h_V} \tag{4}$$

where, A_{int} is the interfacial area concentration, $\mathfrak{H}$ is the heat-transfer coefficient, while h is the specific enthalpy; subscripts L and V denote liquid and vapour phases respectively. To determine the mass transfer, the interfacial area and heat-transfer coefficients are required. The interfacial area is the surface area of the droplets per unit volume (i.e., $A_{int} = 6\alpha_L/D_d$). The droplet mean diameter, D_d, is estimated using the definition of the Weber number We, which relates the disruptive aerodynamic force that acts to fragment the droplet to the surface tension force that resists that fragmentation:

$$We = \frac{\rho_V \, D_d \, |u_V - u_L|^2}{\sigma} \tag{5}$$

where σ is the surface tension. Experimental results indicate that as long as the ratio $\mu_L/\rho_L D_d \sigma$ stays below 0.1 (μ_L is the liquid dynamic viscosity), which is satisfied in all investigated cases, droplet breakup is expected for $We > 11$, in both subsonic and supersonic flow regimes (Guildenbecher, 2009; Gobyzov, 2020). Hence, the maximum stable droplet size can be determined; since no droplet coalescence is simulated, the droplet size decreases or remains constant with increasing streamwise position.

The heat-transfer coefficient on the continuous (vapour) side is evaluated with the Ranz-Marshall (1952) correlation, derived from experimental tests on a water droplet evaporating in a hot air stream. It is more challenging to estimate the heat-transfer coefficient between the droplet and the interface. In previous studies, the authors assumed a constant Nusselt number of 6, which comes from heat-transfer analysis in a solid sphere. Nevertheless, the heat transfer will likely be enhanced in a droplet due to effects such as internal circulation. To predict the heat transfer rate more accurately, a correlation applied in RELAP5/MOD3 (NRC, 1995), a code designed for transient simulation of light water reactor coolant systems, was adapted in this work. The correlation is based on Brown's (1948) work on condensation of water droplets: 306

$$Nu_L = 2 + 7 \times \min\left(1 + \frac{c_{p,L}\max(0, |T_{sat} - T_L|)}{h_{LV}}, 8\right) \tag{6}$$

where Nu_L is the liquid Nusselt number, $c_{p,L}$ is the liquid specific heat capacity at constant pressure, h_{LV} is the latent heat of vapourisation, while T_{sat} is the saturation temperature. This correlation was originally obtained for droplets suspended in a hotter medium. However, the authors assume that similar heat-transfer coefficients can be expected for droplet cooling, and the correlation serves as the current best-estimate.

In the case of the droplet flow, there are three major momentum exchange mechanisms: drag, lift and turbulent dispersion effects, with the first having the highest impact. The drag coefficient is estimated using the Ishii-Zuber (1979) correlation, which was also used in previous simulations. However, the formulations used for the lift and turbulent dispersion forces have been updated in the current work. To evaluate the lift force, the Legendre & Magnaude (1998) is applied, which is more suited to small fluid particles. The previously applied turbulent dispersion model was more suitable for bubbly flow; since liquid droplets are significantly denser than vapour, they are not so easily caught in vapour turbulent eddies. This was accounted for by setting a turbulent dispersion coefficient that depends on the turbulent Stokes number: $c_{TD} = e^{-0.5St_t}$, where c_{TD} is the dispersion coefficient, while St_t is the turbulent Stokes number. In case the droplet relaxation time is much higher than the turbulent eddy lifetime, the droplets will be weakly affected by the eddies. Hence, the turbulent dispersion tends to zero as the turbulent Stokes number increases. Lastly, a suitable equation of state was employed to predict fluid's properties and close the system of equations.

2.2 Quasi-1D Nozzle Design Tool

Two-phase expansion under conditions relevant to the wet-to-dry cycle entails rapid acceleration to supersonic velocities, which leads to significant velocity slip and thermal non-equilibrium that affects the phase change process. Previously, the authors developed a quasi-1D non-equilibrium nozzle design tool, capable of accounting for the non-equilibrium effects. The design tool is based on a simplified version of the two-fluid model described in the preceding section. The flow is assumed to be quasi-1D and inviscid, varying only in the longitudinal direction. Consequently, lift and turbulent dispersion forces are not included.

The nozzle design routine is initiated with the selection of the working fluid and boundary conditions, which include the inlet total pressure and vapour quality alongside inlet velocity. Since the nozzle is intended as a turbine stator integrated with the wet-to-dry cycle, the cycle condensation temperature and the turbine degree of reaction are used to define the nozzle outlet pressure. Previous numerical studies indicate that siloxane MM is a promising candidate for the wet-to-dry cycle, which is why it was selected for the current investigation. The previous results also indicate that a complete wet-to-dry transition can be difficult to achieve when expanding from pressures lower than 750 kPa. On the other hand, the wet-to-dry cycle provides a higher advantage over the single-phase expansion at low pressures. This study aims to undertake optimisation to enhance the evaporation rate at low pressures and consequently enable the design of wet-to-dry turbine at lower pressures. Therefore, three relatively low inlet pressures were considered, namely, 450, 550 and 650 kPa. These pressure levels could correspond to heat source inlet temperature in the approximate range of 170 to 190 °C; temperatures levels where wet-to-dry cycle may provide substantial power output increase (White, 2021). Inlet quality and degree of reaction were set to 0.3 and 0.4 respectively, while the cycle condensation temperature was fixed at 40 °C. The three expansion cases are reported in Fig.1, which shows the ideal isentropic process. Although expanding from lower inlet qualities could offer a further increase in the power output, preliminary turbine design studies have shown that it would require a lower degree of reaction, which could have a detrimental effect on the turbine efficiency (White, 2021). The mass flow rate is set to 0.12 kg/s, which translates to a turbine isentropic power of around 100 to 120 kW under the investigated operating conditions. This power output is estimated assuming that the turbine has sixteen stator vanes; each nozzle representing one stator vane. This power rating could correspond to a small-scale 307
system designed for waste-heat recovery from low-temperature sources. To fully define the nozzle geometry, two geometrical parameters, the ratios of nozzle length to throat height (L/o_{th}), and nozzle width to throat height (b/o_{th}) were set to 30 and 3 respectively (values set in line with former studies).

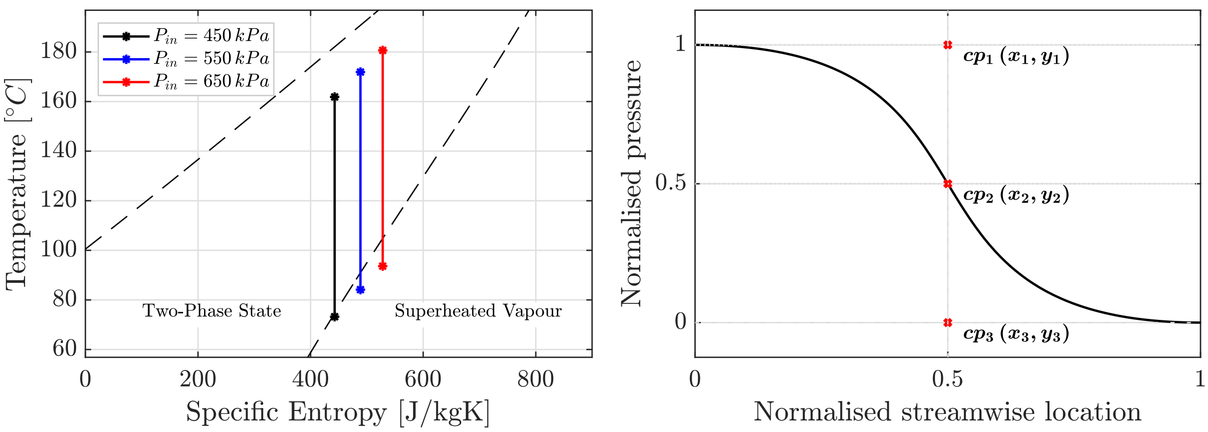

Figure 1: Three investigated expansion cases under isentropic flow assumption (left); normalised baseline pressure profile (right); the red asterisks (*) show the location of the Bezier curve control points.

The quasi-1D tool follows an inverse design approach, where the pressure profile is pre-defined and Eqs. 1-3 are solved to converge on the imposed pressure distribution. NIST REFPROP 10.0 (Lemmon et al., 2018) is employed to evaluate the thermodynamic properties of siloxane MM. Figure 1 illustrates the design pressure profile, which was constructed using a Bezier curve with three control points, cp_1, cp_2 and cp_3, explicitly shown with red markers on the plot. The profile shown is identical to the profile used in all previous investigations and will be referred to as the baseline profile. In this profile, the Bezier control points are positioned such that the pressure gradient approaches zero at the inlet and outlet of the nozzle. Moreover, the pressure at the middle of the nozzle is set to the average of the inlet and outlet pressures.

2.3 Quasi-1D Tool Validation

Before proceeding with the optimisation, the quasi-1D tool has been validated using CFD. Although the validation has already been performed by the authors (Ogrodniczak & White, 2022), several modifications have since been made. Firstly, as highlighted in Section 2.2. the liquid side heat-transfer coefficient, alongside the lift and turbulent dispersion forces, have been updated. A correction to the drag force equation in the quasi-1D tool, which previously caused a discrepancy in the velocity slip, has also been added; the velocity slip directly affects the maximum diameter, which in turn impacts the evaporation rate. Finally, the vapour thermodynamic quality was previously used to measure evaporation rate. However, in the presence of significant non-equilibrium effects, it may be more appropriate to use the vapour mass fraction calculated based on the ratio of vapour to total mass flow rates (i.e., $\dot{m}_V/(\dot{m}_L + \dot{m}_V)$).
The nozzle geometries generated by the tool are assessed through steady-state two-dimensional simulations performed in ANSYS CFX (2021 R1), that accounts for the effects of viscosity and turbulence. REFPROP 10.0 was used to construct look-up tables for the thermo-physical properties of siloxane MM. The maximum droplet diameter formulation was not directly implemented in the CFD. Instead, the streamwise droplet diameter profile extracted from the quasi-1D tool was imposed through a user-defined expression. Direct implementation of Eq. 5 in the CFD solver caused numerical instabilities and hindered convergence. This could be due to excessive droplet size variation in the transverse direction caused by phase separation. As for the grid structure, the authors relied on the previous validation study in determining the appropriate mesh resolution. Nonetheless, it should be mentioned that the grid was improved by constructing a fully structured hexahedral mesh, eliminating low-quality distorted elements. For more details on the numerical setup, the reader is referred to Ogrodniczak & White (2022). Figure 2 presents the updated validation study results.

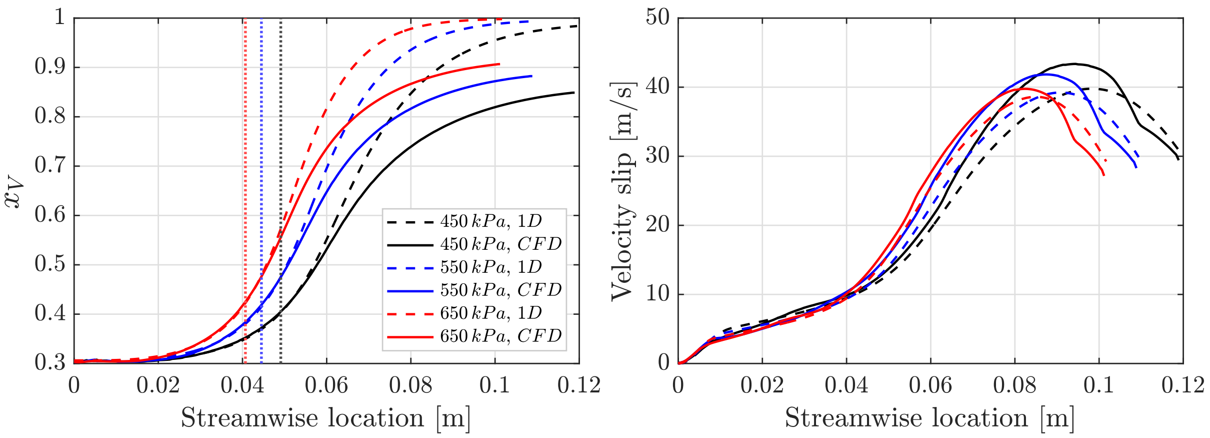

308

Figure 2: Comparison of average streamwise variation of vapour mass fraction (left) and velocity slip (right) between the quasi-1D tool and CFD; the dotted lines represent the throat location.

Figure 2 illustrates the average streamwise variation of vapour mass fraction x_V. The quasi-1D tool predicts near-dry conditions at the nozzle outlet with x_V ranging from 0.984 to 0.998. Most of the phase change occurs shortly past the throat in the diverging nozzle section. The curve then flattens as the flow approaches the outlet. This trend is similar for each of the three expansions; however, the higher the pressure the quicker the evaporation and the higher the outlet vapour quality. Although the CFD predicts a visibly lower evaporation rate compared to the quasi-1D tool, the phase-change pattern looks very similar in both cases. The discrepancy in x_V gradually increases in the diverging section, reaching the maximum of around 0.10–0.15 at the outlet. In summary, the lateral phase separation, viscosity, and turbulence effects are likely to delay the evaporation and lead to increased liquid content in the nozzle outflow.

In the previous study, the velocity slip estimated by the quasi-1D tool was significantly smaller than the CFD predictions. With the corrected drag formulation, the velocity slip difference is reduced from a maximum of 38 m/s to less than 5 m/s (Fig. 2). Overall, the slip predicted by the quasi-1D tool is now much higher, which translates to smaller droplet size in the nozzle diverging section and higher evaporation rates (Eqs. 4-6). Despite the quantitative differences between the design tool and the CFD, the overall phase change pattern is conserved. Therefore, it seems rational to assume that enhancing the evaporation rate in the quasi-1D tool will translate to enhanced evaporation in the CFD. This justifies using the quasi-1D tool for optimisation.

3 PRESSURE PROFILE OPTIMISATION

3.1 Optimisation Setup

As apparent from Fig. 2, achieving complete mixture evaporation at pressures below 650 kPa is challenging. This study aims to enhance evaporation by optimising the nozzle pressure distribution to assess whether complete evaporation could be achieved in low-pressure expansions. A nonlinear constrained optimisation is setup using the gradient-based *fmincon* optimiser available within MATLAB. Since it was found that multiple pressure profiles resulted in complete evaporation, the objective function was defined as:

$$f(\mathbf{x}) = \mathrm{x}_{\mathrm{V,max}} \frac{L_N}{L\ @\ x_{V,\max}} \tag{7}$$

where $\mathrm{x}_{\mathrm{V,max}}$ is either 1 in case of full evaporation or the maximum vapour mass fraction achieved, L_N is the nozzle length, and $L\ @\ x_{V,\max}$ is the streamwise distance at which the mixture turns to dry vapour or reaches the maximum x_V. Maximising $f(\mathbf{x})$ ensures that a pressure profile is found that ensures the quickest wet-to-dry transition. The design variables are the coordinates of the three Bezier control points shown in Fig. 1. Although it was initially planned to include the geometrical ratios, L/o_{th} and b/o_{th} as design variables, both parameters were found to have little effect on the evaporation rate. To avoid flow discontinuities, the zero-gradient condition is maintained at the inlet and outlet, which implies that the y-coordinate of the control points cp_1 and cp_3 is fixed at 1 and 0 respectively. Hence, there are four design variables in total, which include the x-coordinates of all three control points, and the y-coordinate of the middle control point cp_2. Each design variable can take any value between 0 and 1 in terms of the normalized coordinates (see Fig. 1). However, the resulting profile has to satisfy two conditions (optimisation constraints). First, the pressure gradient dp/dx has to remain negative throughout the expansion, i.e. the pressure had to continually decrease. The other constraint was related to the maximum magnitude of the pressure gradient $|dp/dx|$, which could not exceed 25 (expressed in terms of normalised coordinates). It was found that pressure profiles with $|dp/dx| > 25$ resulted in excessive nozzle curvature. This in turn led to very abrupt expansions associated with flow separation. To avoid ending up at a local minimum, the optimiser was run using 100 randomly generated starting points within the design space.

3.2 Optimisation results

Figure 3 presents the comparison between the baseline and optimised pressure profiles. In each case, the optimum pressure profile reaches the maximum allowable gradient of 25. The profiles for 550 and 650 kPa expansions look almost identical, with most of the expansion happening closer to the inlet. This seems logical as the breakup occurs quicker, with the remaining of the expansion occurring with smaller droplets. It is unclear why the pressure drop occurs further downstream for the 450 kPa expansion. The main reason why the optimiser strove to maximise the pressure gradient and bring about a more rapid expansion is that it promotes a more severe droplet fragmentation and leads to smaller droplet diameters in the diverging section of the nozzle. The post-breakup droplet diameter in nozzles designed with the baseline profile varied between 10.4 and 13.2 μm. This reduced to around 4.34 to 5.57 μm in the optimised nozzles. The smaller the droplet size the larger the interfacial area for a given liquid volume fraction; this in turn directly enhances the rate of interfacial heat transfer rate and consequently interphase mass transfer. According to the quasi-1D tool, the optimised geometry provides dry outlet conditions in each case and wet-to-dry transition took place further upstream of the outlet compared to the baseline profile (compare dashed line in Fig. 2 and Fig. 3). In order to test whether the enhanced evaporation rate was merely the result of reduced droplet size, the design was repeated for the baseline and optimised profiles using a constant droplet diameter of 15 μm. Even though the droplet diameter remained constant, the evaporation was enhanced, which indicates there are other mechanisms involved in raising the evaporation rate when the pressure gradient is increased.

Although the quasi-1D results look promising, the evaporation may be reduced by the two-dimensional, viscosity and turbulence effects as apparent from Fig. 2. Figure 3 shows the comparison between quasi-1D and CFD predictions of average streamwise x_V for the optimised pressure profiles. First, comparing Fig. 3 to Fig. 2, it can be easily noticed that like in the baseline cases, the evaporation rate estimated by CFD is reduced in comparison with the quasi-1D tool prediction, while the overall trends are conserved. Comparing the CFD results of the baseline and optimised geometries (Fig. 4), a visible and consistent improvement in the outlet vapour mass fraction can be observed, which amounts to around 0.055 to 0.066. The outlet x_V increases from 0.849, 0.882 and 0.907 to 0.904, 0.948 and 0.972 for the 450, 550 and 650 kPa expansions respectively. Although full evaporation was not achieved in any of the investigated cases, the liquid mass fraction at the outlet of the optimised nozzle design for the expansion from 650 kPa dropped below 3%, which is promising. Considering the gradient of the x_V curve near the outlet, it appears that further increase in the outlet x_V could be achieved by elongating the nozzle.

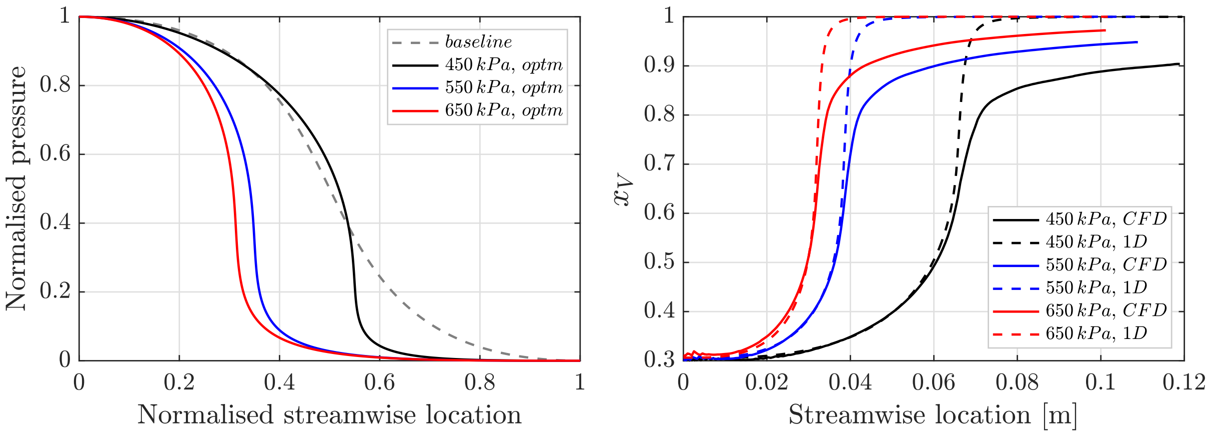

Figure 3: Optimised pressure profiles (left); Comparison of average streamwise variation of vapour mass fraction x_V predicted by the quasi-1D tool and CFD in the optimised geometries.

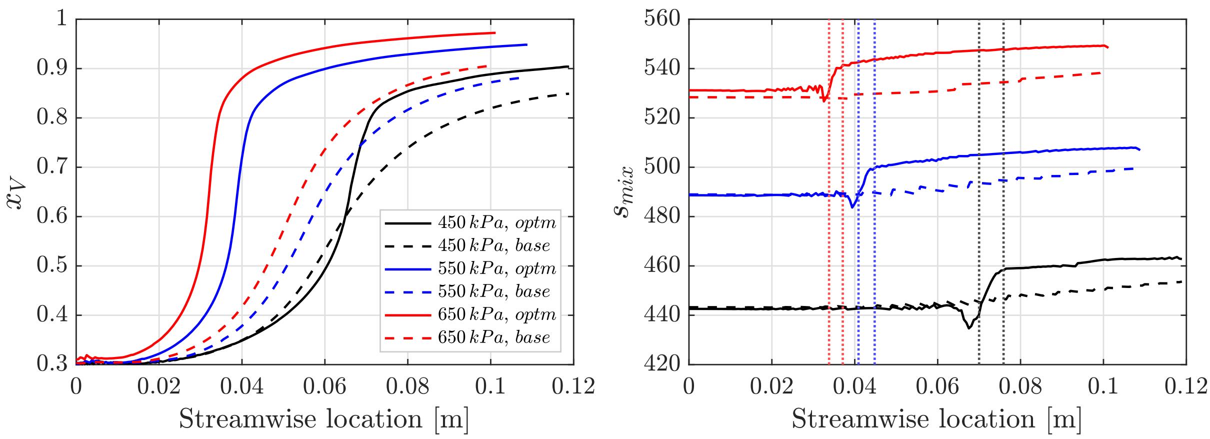

Figure 4: Comparison of CFD predictions of average streamwise variation of a) vapour mass fraction and b) mass-flow average entropy for the baseline (*base*) and optimized (*optm*) pressure profiles; dotted lines represent the nozzle sections with the most sudden entropy increase.

The influence of the pressure profile on the nozzle efficiency and flow uniformity is also important. Figure 4 reports the average streamwise variation of mass-flow averaged entropy (s_{mix}). Generally, the more rapid pressure change that results in the optimised case has a negative effect on the nozzle performance as the total entropy generated increases. One can note a small kink in the entropy curves, showing a local decrease in total entropy in the throat area, which would not happen in any real process. However, as entropy immediately rises after, it is thought that overall the results remain valid. To provide a more explicit measure of nozzle performance, nozzle efficiency was calculated, based on the ratio of actual to isentropic kinetic energy rise. The efficiency of the baseline nozzles was 80.97, 82.76 and 84.39% for the 450, 550 and 650 kPa expansion respectively. The efficiency dropped to 72.37, 78.43 and 82.11% for the optimised geometries, which is in line with the total entropy curves (Fig. 4).

Figure 5 shows 2D vapour mass fraction contours, which reveal the flow's spatial uniformity, shedding more light on flow behaviour and the cause for the sudden rise in generated entropy. What appears to be common in each case, is the phase separation in the diverging section of the nozzle. This is due to much higher liquid density and high relaxation times; the droplets cannot immediately adjust to the changing geometry in an accelerating flow field. For that reason, the liquid tends to remain in the centre of the nozzle past the throat, while the vicinity of the wall is occupied by the vapour phase. The flow-field looks very similar in each baseline geometry. Comparing the baseline and optimised nozzles, the phase separation in the diverging section seems to be alleviated in the optimised geometries. Nevertheless, an oblique shock appears to form in the optimised nozzles shortly downstream of the throat, which eventually causes entropy generation and performance loss. The dotted lines from Fig. 4 also shown on the contours, indicate where the sudden entropy generation occurs in the nozzle. It can be observed that the location of the sudden rise in s_{mix} can be linked to the onset of the shock. Looking at the optimised geometries, the most abrupt flow area change occurs for the 450 kPa expansion, the area change gradually decreases as the inlet pressure is raised. This is also the reason why the shock is stronger for the 450 kPa expansion, resulting in a more pronounced efficiency loss; over 8% lower efficiency compared with slightly over 2% loss for the 650 kPa expansion. In summary, the optimised geometry can provide higher outlet vapour mass fraction and reduces the extent of lateral phase separation in the diverging section. However, more abrupt expansion can induce shocks and consequently performance losses. The influence of the multidimensional and viscosity effects on the nozzle performance highlights the limitation of the 1D optimisation, which can only be applied to maximise the evaporation rate. CFD-based nozzle shape optimisation could be applied to perform multi-objective optimisation, aimed at enhancing the evaporation rate while maintaining high nozzle efficiency. It is also important to note that all the investigated nozzles have a straight centerline. For a curved deflecting nozzle, one could expect that phase separation would be enhanced due to lateral gradients. Most likely, liquid phase would concentrate on the pressure side of the nozzle, creating a characteristic liquid film as found by Rane & He (2020). Such phase separation would lead to a reduced interfacial area A_{int}, which in turn lowers the interphase mass exchange rate and delays the evaporation (see Eq. 4). The phase separation could also decrease the uniformity of flow delivered by the nozzle. In summary, the design of a curved (deflecting) nozzle that would facilitate complete mixture evaporation and uniform outlet flow conditions is likely to be more challenging.

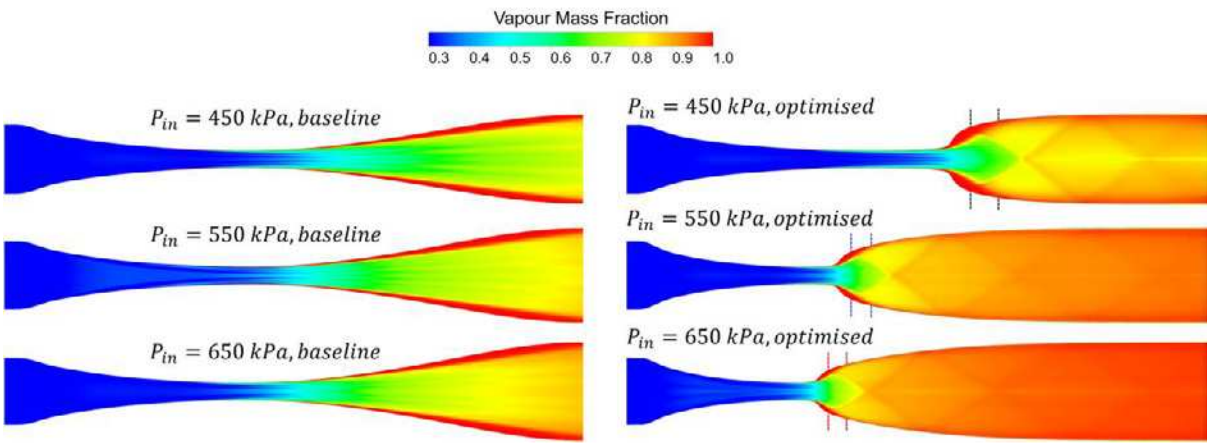

Figure 5: Two-dimensional contours of vapour mass fraction in the baseline and optimised geometries; dotted lines correspond to the location of the most sudden entropy increase.

4 CONCLUSIONS

Pressure profile optimisation was conducted in this study, using a CFD-validated quasi-1D non-equilibrium design tool, capable of generating nozzle geometries for the wet-to-dry expansion of organic vapours. Three expansions with inlet pressure ranging from 450 to 650 kPa and constant inlet vapour quality of 0.3 were investigated for the siloxane MM. It was found that the quasi-1D nozzle design tool is capable of predicting the phase-change pattern, but the assumption of inviscid quasi-1D flow and the omission of viscous and turbulence effects leads to an overprediction in the evaporation rate. However, since the phase-change pattern predicted by the quasi-1D tool is similar to the CFD predictions, the tool was still deemed suitable for performing 1D optimisation. Optimised geometries were simulated using a CFD model that accounted for viscosity, turbulence and two-dimensional effects. It was found that the optimised nozzles resulted in a rapid expansion that enhanced the evaporation rate. The CFD simulations conducted on the geometries generated using the optimised pressure profile achieved between 5.5 to 6.6% higher vapour mass fraction at the outlet, which reached 90.4, 94.8 and 97.2% for the expansions from 450, 550 and 650 kPa respectively. Although complete evaporation was achieved in none of the cases, reaching near-dry conditions for inlet pressures in the order of 650 kPa seems promising. Evaluation of the flow-field revealed that the abrupt expansion in the optimised geometries was associated with the formation of an oblique shock downstream of the throat, which in turn contributed to elevated entropy generation. The nozzle efficiencies for the optimised geometries were approximately 2 to 8% lower compared to the baseline geometries, with more pronounced loss at low pressures. This highlights the limitation of the 1D optimisation and emphasises the need for multi-objective CFD-based shape optimisation to maximise outlet vapour mass fraction whilst minimising performance loss.

REFERENCES

Brown, G., 1948, "*Heat transmission by condensation of steam on a spray of water drops"*, PhD thesis, University of London (Imperial College of Science and Technology).

Gobyzov, O. A., M. N. Ryabov, and A. V. Bilsky, 2020, "Study of Deformation and Breakup of Submillimeter Droplets' Spray in a Supersonic Nozzle Flow", *Applied Sciences,* 10(18), p. 6149.

Guildenbecher, D. R., Lopez-Rivera, C., and Sojka, P. E., 2009, "Secondary atomization", *Experiments in Fluids,* 46(3), pp. 371–402.

Ishii, M. and N. Zuber, 1979, "Drag coefficient and relative velocity in bubbly, droplet or particulate flows", *AIChE Journal.* 25(5), pp. 843–855.

312

Legendre, D. and Jacques M., 1998, "The lift force on a spherical bubble in a viscous linear shear flow", *Journal of Fluid Mechanics,* 368, pp. 81–126.

Lhermet, G., Tauveron, N., Caney, N., Blondel, Q., Morin, F., 2022, "A Recent Advance on Partial Evaporating Organic Rankine Cycle: Experimental Results on an Axial Turbine", *Energies,* 15(20), p. 7559.

Lemmon, E. W. et al. (2018). NIST Standard Reference Database 23: Reference Fluid Thermodynamic and Transport Properties-REFPROP, Version 10.0, National Institute of Standards and Technology.

NRC - US Nuclear Regulatory Commission, 1995, "RELAP5/MOD3 Code Manual. Volume 4: Models and correlations", Tech. rep, Idaho National Engineering Laboratory.

Ogrodniczak, P. and White, M.T., 2022, "Numerical validation of a two-phase nozzle design tool based on the two-fluid model applied to wet-to-dry expansion of organic fluids", *4th International Seminar on Non-Ideal Compressible Fluid Dynamics for Propulsion and Power,* 3-4th November, London, UK.

Ogrodniczak, P. and White, M.T., "Non-equilibrium CFD simulation of the wet-to-dry expansion of the siloxane MM in a converging-diverging nozzle", *Applied Thermal Engineering,* [Under review].

Rane, S. and He L., 2020, "CFD analysis of flashing flow in two-phase geothermal turbine design", *Journal of Computational Design and Engineering,* 7(2), pp. 238–250.

Ranz, W. E. and W. R. Marshall Jr., 1952, "Evaporation from Drops: Part 1", *Chemical Engineering Progress*, 48(3), pp. 141–146.

White, Martin T., 2021, "Cycle and turbine optimisation for an ORC operating with two-phase expansion", *Applied Thermal Engineering*, 192, p. 116852.

White, Martin T., 2022, "Investigating the wet-to-dry expansion of organic fluids for power generation", *International Journal of Heat and Mass Transfer*, 192, p. 122921.

Wieland, C., Schifflechner, C., Braimakis, K., Kaufmann, F., Dawo, F., Karellas, S., Besagni, G., Markides, C.N., 2023, "Innovations for organic Rankine cycle power systems: Current trends and future perspectives", *Applied Thermal Engineering*, 225, p. 120201.

This book contains the compilation of works contributed to the *7th International Seminar on Organic Rankine Cycle Power Systems* (ORC 2023), held in Seville between the 4th and 6th of September 2023. The event was hosted by Universidad de Sevilla on behalf of the Knowledge Centre on Organic Rankine Cycle Technology (KCORC), incorporated in The Netherlands.

The ORC conference, organized biennially, stems as the only conference that is specific to ORC technology, therefore gathering a diverse community whose affiliation spans across all the interested stakeholders, not only in this particular technology but also and in a broader context, in the energy transition. Original equipment manufacturers, professional associations, end-users, investors, policy makers, academics, scientists feel at home at ORC 2023.

The almost 100 proceedings in this book cover a wide variety of topics, from fundamentals to system integration through component design, accounting for thermodynamic performance as well as component design. In addition to this, and as a new track in 2023, works on heat pump technology were also accepted in order to raise awareness of the strong ties between both technologies, specifically in energy storage applications.

This book provides an excellent overview of the current maturity of power systems based on Organic Rankine Cycle technology for applications as diverse as geothermal and waste heat recovery in industry or downstream of other prime movers (e.g., marine applications). It is also an excellent source of information to understand the current challenges faced by the technology, stemming from a very competitive market and increasingly stringent environmental regulations.

The organizers of ORC 2023 hope that the reader finds this work as exciting as the attendees to the conference and, maybe, make the decision to join the 8th edition to the conference in 2025.

KCORC
KNOWLEDGE CENTER
ORGANIC RANKINE CYCLE

eUS EDITORIAL
UNIVERSIDAD DE SEVILLA